

# Dynamic actin/septin network in megakaryocytes coordinates proplatelet elaboration

Isabelle C. Becker,<sup>1,2\*</sup> Adrian R. Wilkie,<sup>1,2\*</sup> Bret A. Unger,<sup>3</sup> Anthony R. Sciaudone,<sup>4</sup> Farheen Fatima,<sup>1,2</sup> I-Ting Tsai,<sup>1,2</sup> Ke Xu,<sup>3</sup> Kellie R. Machlus<sup>1,2</sup> and Joseph E. Italiano Jr<sup>1,2</sup>

<sup>1</sup>Vascular Biology Program, Boston Children's Hospital, Boston, MA; <sup>2</sup>Department of Surgery, Harvard Medical School, Boston, MA; <sup>3</sup>Department of Chemistry, University of California, Berkeley, CA and <sup>4</sup>Brigham and Women's Hospital, Boston, MA, USA

*\*ICB and ARW contributed equally as first authors.*

**Correspondence:** J. Italiano  
[joseph.italiano@childrens.harvard.edu](mailto:joseph.italiano@childrens.harvard.edu)

**Received:** April 19, 2023.

**Accepted:** August 18, 2023.

**Early view:** September 7, 2023.

<https://doi.org/10.3324/haematol.2023.283369>

©2024 Ferrata Storti Foundation

Published under a CC BY-NC license



## **Dynamic actin/septin network in megakaryocytes co-ordinates proplatelet elaboration**

\*Isabelle C. Becker<sup>1,2</sup>, \*Adrian R. Wilkie<sup>1,2</sup>, Bret A. Unger<sup>3</sup>, Anthony R. Sciaudone<sup>4</sup>, Farheen Fatima<sup>1,2</sup>, I-Ting Tsai<sup>1,2</sup>, Ke Xu<sup>3</sup>, Kellie R. Machlus<sup>1,2</sup>, Joseph E. Italiano Jr.<sup>1,2</sup>

<sup>1</sup>Vascular Biology Program, Boston Children's Hospital, 1 Blackfan Circle, Boston, MA, 02115;

<sup>2</sup>Department of Surgery, Harvard Medical School, 25 Shattuck Street, Boston, MA 02115;

<sup>3</sup>Department of Chemistry, University of California, Berkeley, Berkeley, CA, 94720; <sup>4</sup>Brigham and Women's Hospital, 4 Blackfan Circle, Boston, MA, 02115

\*Authors contributed equally.

Correspondence to Joseph Italiano: [joseph.italiano@childrens.harvard.edu](mailto:joseph.italiano@childrens.harvard.edu)

## **Supplemental Methods**

### **Platelet depletion**

Mice were injected with 2 µg/g of a platelet depletion antibody (#R300, Emfret Analytics) or an antibody control (C301, Emfret Analytics). Platelet counts were analyzed before and after depletion at an automated blood cell analyzer (Sysmex). After 72h, mice were sacrificed by CO<sub>2</sub> asphyxiation femurs were retrieved for further analysis.

### **Cryosectioning and immunofluorescence staining**

Femora were fixed in 4% PFA/PBS overnight, after which a sucrose gradient was performed. After 3 days, femora were embedded and sectioned at 10 µm using a tape transfer system.<sup>1</sup> Sections were rehydrated in PBS for 20 min, blocked using 10% goat serum and stained for Sept2 (PA5-53814, Invitrogen), Sept5 (PA5-31212, Invitrogen), Sept7 (13818-1-AP, Proteintech) or Sept9 (10769-1-AP, Proteintech), F-actin (Phalloidin Atto647N, 65906, Sigma Aldrich) and β1-tubulin (GTK107175, GeneTex). Nuclei were distinguished using DAPI. Representative images were acquired at a Zeiss LSM880 confocal microscope (40x objective). Colocalization analysis was performed using the JACoP Plugin in ImageJ for several MKs per field of view.

### **Isolation of murine fetal liver and bone marrow MKs**

Fetal liver cells were retrieved from embryos of pregnant CD-1 mice and cultured in DMEM containing 50 ng mL<sup>-1</sup> TPO as indicated.<sup>2</sup> Bone marrow was isolated from femora, tibiae, iliac crests and humeri by centrifugation for 40 seconds at 2500 x g.<sup>3</sup> Cells were labeled using a biotin rat anti-mouse lineage panel (133307, BioLegend) and magnetically retrieved using anti-rat Dynabeads™ (11415D, ThermoScientific). Lineage-depleted progenitors were cultured in TPO-containing DMEM for 72h. To enhance proplatelet formation, bone marrow cells were cultured in the presence of 100 anti-thrombin units (ATU) recombinant hirudin (ARE120A, Aniara Diagnostic). Cells matured for 4 days, after which a density gradient enrichment was performed as previously described.<sup>2</sup>

### **Retroviral expression of fluorescent proteins in fetal liver-derived MKs**

Fetal liver-derived progenitor cells were transduced with murine stem cell virus LifeAct-mRuby (MSCV-LifeAct-mRuby) or MSCV-β1-tubulin-dendra2 as previously published,<sup>4</sup> and cultured in media containing 50 ng mL<sup>-1</sup> TPO until day 4.

### **Live-cell imaging of proplatelet formation and movement**

Fetal liver-derived MKs were isolated as described above. For Incucyte analysis, MKs were treated with LatA (L12370, Invitrogen), CytoD (PHZ1063, Invitrogen), CK666 (HY-16926, MedChemExpress), SMIFH2 (4401, TOCRIS), CASIN (HY-12874, MedChemExpress) or FCF (HY-B1841, MedChemExpress) immediately following density gradient enrichment at the indicated concentrations and proplatelet formation was visualized on an Incucyte imaging system and quantified using a custom image analysis pipeline.<sup>5</sup> For movement analysis, released proplatelets were treated with vehicle or the indicated inhibitors (10 µM LatA or 100 µM FCF), embedded in methylcellulose, and imaged using a Lionheart FX imaging system. Analysis of proplatelet movement was conducted using the Difference Track macro in ImageJ (Version 2.1.0/1.53c). MKs transduced with MSCV-LifeAct-mRuby were enriched by density gradient

sedimentation<sup>2</sup> and F-actin structures were imaged using live cell spinning-disk confocal microscopy prior to proplatelet formation or during proplatelet formation as indicated (Yokogawa spinning disk confocal on an inverted Nikon Ti fluorescence microscope with incubation enclosure; 20x objective). Alternatively, MKs were enriched and treated with vehicle, 1  $\mu$ M LatA or 100  $\mu$ M FCF for 5h. 1h prior to imaging F-actin was stained using 500 nM SiR-Actin (CY-SC001, Cytoskeleton, Inc). Live-cell imaging of F-actin dynamics was performed by confocal microscopy (Zeiss LSM880, 40x objective).

### **Bioreactor**

Fetal liver or bone marrow MKs were isolated as described previously and seeded into a custom-made bioreactor previously published by our laboratory.<sup>6</sup> MKs were imaged every 5 seconds on Nikon widefield microscope as they produced proplatelets for 30 mins before syringe feeding side channels was swapped for a syringe containing media with 30  $\mu$ M LatA (to achieve a final concentration of 10  $\mu$ M in the chip). Proplatelet-producing MKs treated with LatA were imaged every 5 seconds for 30 mins as before. Proplatelet tip positions were measured using the manual Tracker macro in ImageJ (Version 2.1.0/1.53c) and mean proplatelet tip velocities were calculated from tracking data.

### **Kymographs**

Fetal liver-derived MKs were transduced with an MSCV-GFP construct as described before and isolated on day 4. Mature MKs were allowed to make proplatelets for 24 hours before being subjected to a second BSA gradient. The 1% BSA fraction containing released proplatelets was removed and treated with indicated inhibitors, embedded in methylcellulose, and imaged with live cell confocal microscopy (Yokogawa spinning disk confocal on an inverted Nikon Ti fluorescence microscope with incubation enclosure; 20x objective). Proplatelet movement was analyzed by monitoring changes in fluorescence localization over a 4-hour time course using kymographs.

### **Flow cytometry on mature MKs**

Bone marrow-derived MKs were cultured as described above. Whole cultures were retrieved on day 4, spun down and stained for CD41 (133904, Biolegend) and CD42d (148504, Biolegend) on ice for 30 min. Percentage of positive cells was assessed by flow cytometry (BC Accuri).

### **Immunofluorescence staining of proplatelet-forming MKs/MKs in solution**

Fetal liver- or bone marrow-derived MKs were differentiated as described above. Density gradient separation was performed on early day 4 and enriched MKs were incubated for 24h on CD31-coated (102502, Biolegend) 8-well coverglass chambers (155409, ThermoFisher Scientific) in the presence of 10  $\mu$ M LatA, 20  $\mu$ M CASIN or 100  $\mu$ M FCF. MKs were fixed using 4% PFA/PBS containing 0.1% Tween20 and non-specific antibody binding was blocked using 3% BSA/PBS. Cells were stained for Sept2 (PA5-53814, Invitrogen), Sept5 (PA5-31212, Invitrogen), Sept7 (13818-1-AP, Proteintech) or Sept9 (10769-1-AP, Proteintech), F-actin (Phalloidin Atto647N, 65906, Sigma Aldrich) and  $\alpha$ -tubulin-AlexaFluor488 (MA1-38000-A488, Invitrogen). Number of proplatelet and proplatelet tips were counted manually using the cell counter plugin in ImageJ. F-actin density was analyzed by using the threshold plugin in ImageJ; F-actin-rich areas are shown as a percentage of the total cell area. MKs in solution were resuspended in media after density gradient enrichment and were treated with DMSO, 20  $\mu$ M CASIN or 100  $\mu$ M FCF. Cells were fixed

in 4% PFA/PBS containing 0.1% Tween20 24h later. MKs were stained for F-actin and GPIX (clone 56F8<sup>7</sup>). Nuclei were counterstained using DAPI. Images were acquired at a Zeiss LSM880 (63x objective). Colocalization analysis was performed using the JACoP Plugin in ImageJ using three representative cells per condition.

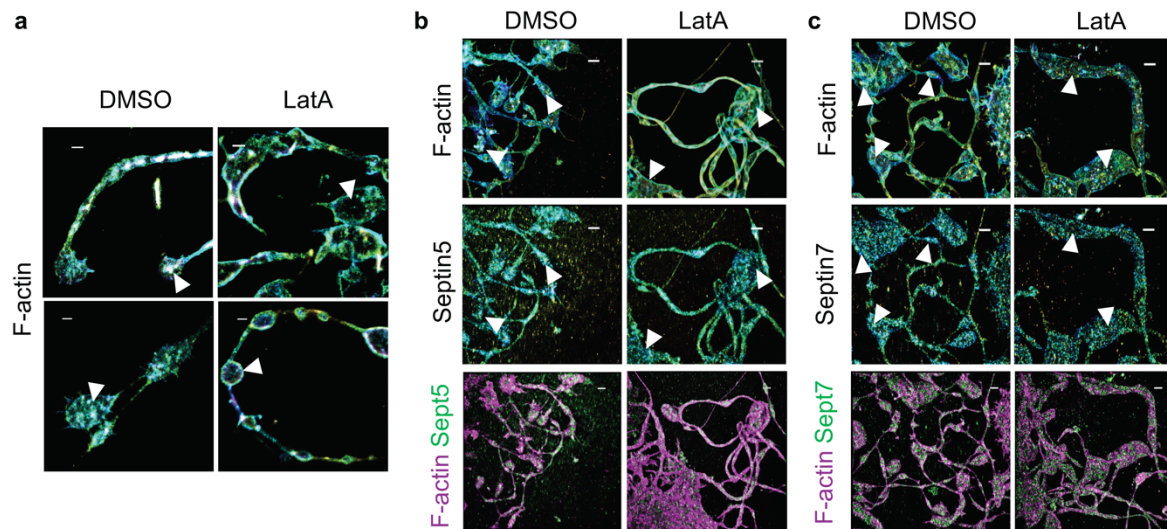
### **Fluorescence recovery after photobleaching (FRAP)**

Fetal liver-derived MKs were transduced with MSCV- $\beta$ 1-tubulin-dendra2 as described above and isolated using density gradient enrichment. Mature MKs were allowed to make proplatelets for 24 hours before being subjected to a second BSA gradient. The 1% BSA fraction containing released proplatelets was removed, treated with the indicated inhibitors (10  $\mu$ M Taxol or 10  $\mu$ M LatA) and embedded in methylcellulose. FRAP was conducted by bleaching proplatelet regions with a 405 nm laser and imaging of the FITC channel every second for 1 minute. Fluorescence was measured and used to calculate corrected intensity for each timepoint.

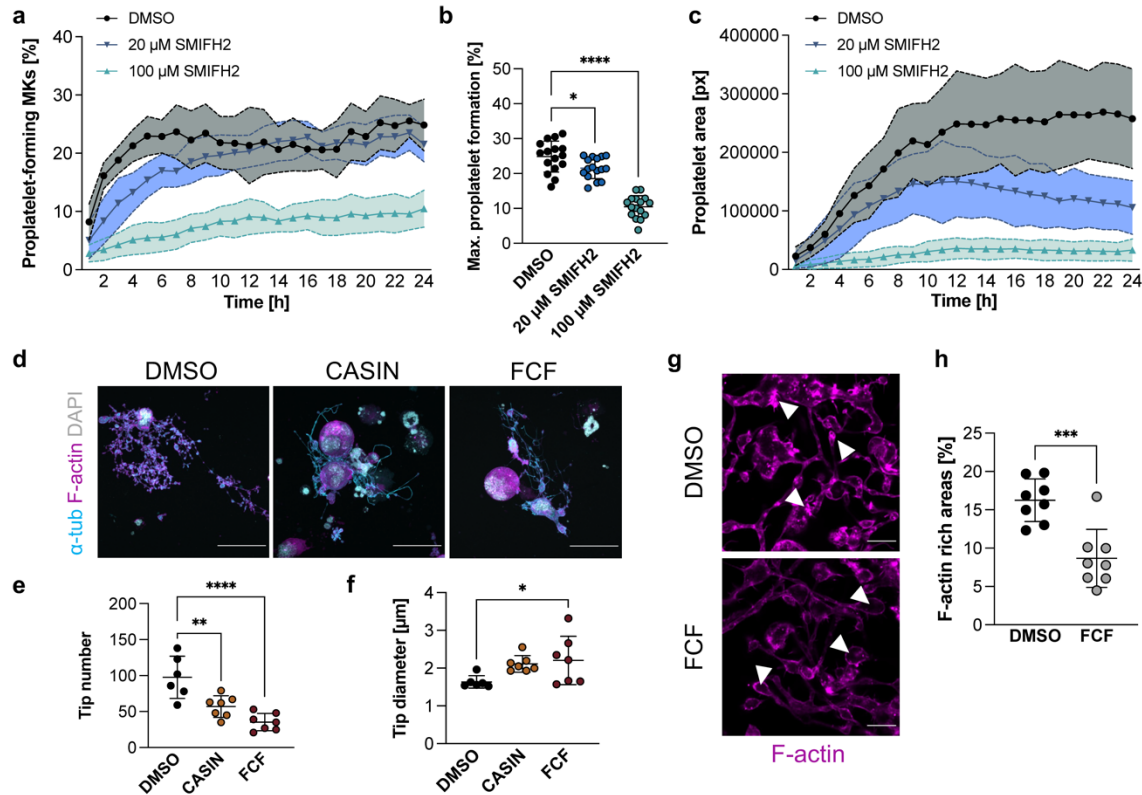
### **Three-dimensional stochastic optical reconstruction microscopy (3D-STORM)**

Proplatelet-forming MKs were prepared as described above and treated with DMSO or 1  $\mu$ M LatA for 24h. Cells were fixed in 3% PFA and 0.1% GA for 30 min, then washed twice with 0.1% NaBH<sub>4</sub> and stored in PBS afterwards. 3D-STORM<sup>8,9</sup> was carried out on a home-built set-up using a Nikon CFI Plan Apo  $\lambda$  100x oil immersion objective (NA 1.45), described in previous work.<sup>10</sup> The sample was mounted with an imaging buffer consisting of 5% (w/v) glucose, 100 mM cysteamine, 0.8 mg ml<sup>-1</sup> glucose oxidase and 40  $\mu$ g ml<sup>-1</sup> catalase in a Tris HCl buffer (pH 7.5). For two-color imaging, the targets were labeled with primary antibodies (Sept5 (PA5-31212, Invitrogen) and Sept7 (13818-1-AP, Proteintech)), followed by labelling with Phalloidin-AF647 and anti-rabbit-CF568 (Jackson ImmunoResearch 711-005-152), and were imaged sequentially using 647- and 560-nm excitation lasers. These lasers were passed through an acousto-optic tunable filter and illuminated a few  $\mu$ m into the sample at around 2 kW cm<sup>-2</sup>, thus photoswitching most of the labeled dye molecules in the sample into the dark state while allowing a small, random fraction of molecules to emit across the wide-field over different camera frames. Single-molecule emission was passed through a cylindrical lens of focal length 1 m to introduce astigmatism,<sup>8</sup> and recorded with an Andor iXon Ultra 897 EM-CCD camera at a frame rate of 110 Hz, for a total of around 50,000 frames per image. Data acquisition used publicly available software (<https://github.com/ZhuangLab/storm-control>). The raw STORM data were analysed using Insight3 software<sup>8</sup> according to previously described methods.<sup>8,9</sup>

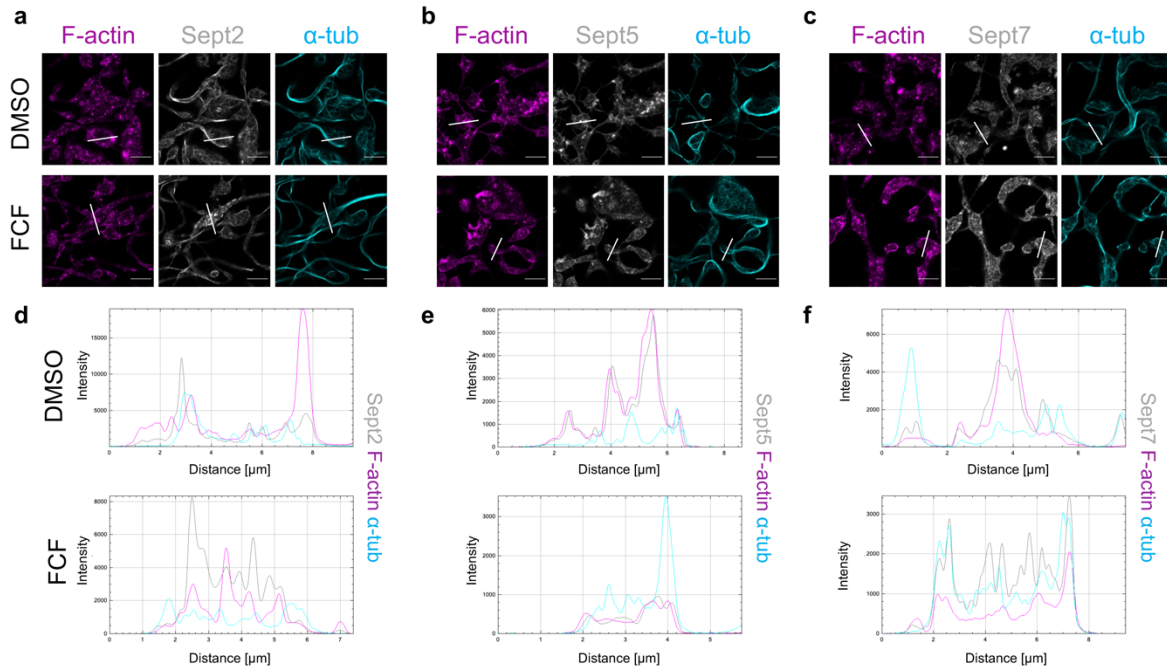
## Supplemental Figure Legends



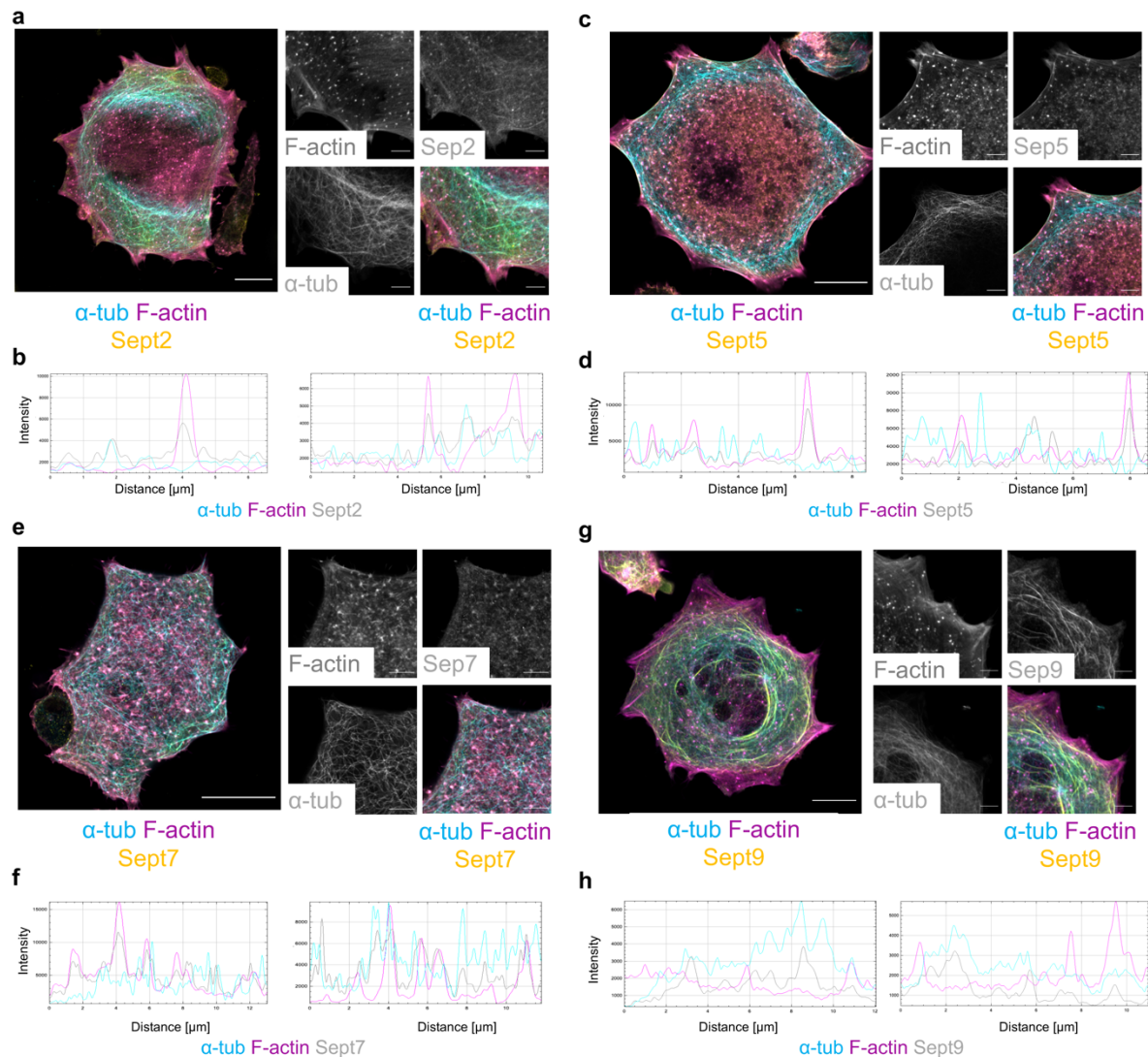
**Supplemental Figure 1. Super-resolution microscopy reveals impaired intracellular F-actin dynamics upon LatA treatment.** (a) Visualization of F-actin in bone marrow-derived proplatelet-forming MKs upon DMSO or LatA-treatment (1  $\mu$ M). Scale bars: 1  $\mu$ m. (b, c) F-actin and Sept7 (b) or Sept5 (c) were visualized in bone marrow-derived proplatelet-forming MKs using 3D stochastic optical reconstruction microscopy (3D-STORM). Scale bars: 2  $\mu$ m. Arrows highlight actin/septin accumulations.



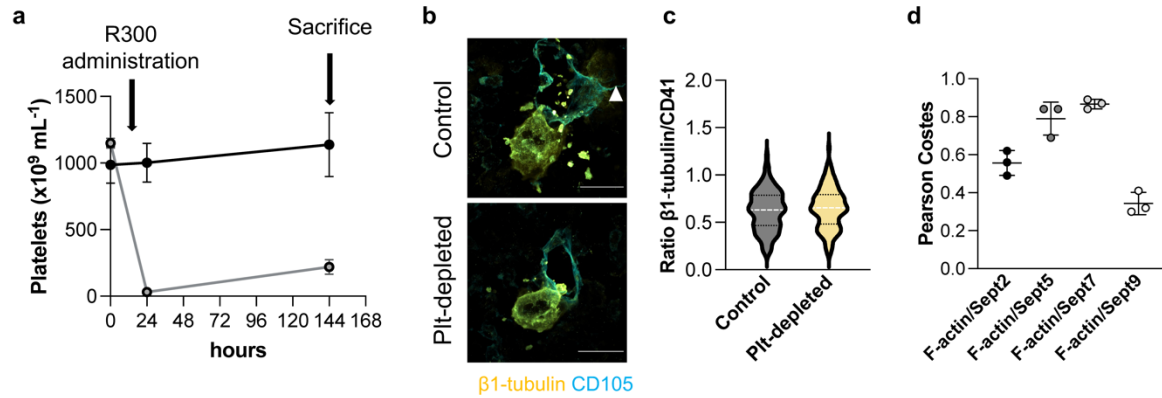
**Supplemental Figure 2. Cdc42/septin/formin inhibition impairs intracellular F-actin dynamics.** (a - c) Fetal liver-derived MKs were treated with the indicated concentrations of the formin inhibitor SMIFH2 and imaged for 24 hours using an Incucyte imaging system. Percentage of proplatelet-forming MKs (a, b) and proplatelet area (c) were analyzed using a custom imaging pipeline. N = 2 mice. 3 technical repeats. Data is presented as mean ± SD. One-way ANOVA with Sidak correction for multiple comparisons. P < 0.05 \*; p < 0.0001 \*\*\*\*. (d) Immunofluorescence staining for F-actin and α-tubulin of bone marrow-derived proplatelet-forming MKs treated with DMSO, CASIN or FCF. Scale bars: 50 μm. (e, f) Quantification of proplatelet tip size and number in MKs treated with DMSO, 20 μM CASIN or 100 μM FCF. Data is presented as mean ± SD. One dot represents one cell. N = 3. One-way ANOVA with Sidak correction for multiple comparisons. P < 0.05 \*; p < 0.01 \*\*; p < 0.0001 \*\*\*\*. (g, h) Visualization (g) and quantification (h) of F-actin-rich areas in bone marrow-derived proplatelet-forming MKs. Scale bars: 5 μm. Data is presented as mean ± SD. One dot represents one cell. N = 3. Unpaired, two-tailed student's t-test. P < 0.001 \*\*\*.



**Supplemental Figure 3. The septin cytoskeleton in fetal liver-derived MKs. (f - h)** Visualization of F-actin,  $\alpha$ -tubulin and Sept2 (d), Sept5 (e) and Sept7 (f) in fetal liver-derived proplatelet-forming MKs upon DMSO- or FCF-treatment. Scale bars: 5  $\mu$ m. (i - k) Line plots showing overlay of F-actin, septins and  $\alpha$ -tubulin in DMSO- and FCF-treated MKs.



**Supplemental Figure 4. Distinct localization of different septin classes to F-actin or microtubules.** (a, b) Visualization (a) and two line plots (b) of F-actin,  $\alpha$ -tubulin and Sept2 in bone marrow-derived MKs spread on fibrinogen. Scale bars: 15  $\mu$ m; insets: 5  $\mu$ m. (c, d) Visualization (c) and two line plots (d) of F-actin,  $\alpha$ -tubulin and Sept5 in bone marrow-derived MKs spread on fibrinogen. Scale bars: 15  $\mu$ m; insets: 5  $\mu$ m. (e, f) Visualization (e) and two line plots (f) of F-actin,  $\alpha$ -tubulin and Sept7 in bone marrow-derived MKs spread on fibrinogen. Scale bars: 15  $\mu$ m; insets: 5  $\mu$ m. (g, h) Visualization (g) and two line plots (h) of F-actin,  $\alpha$ -tubulin and Sept9 in bone marrow-derived MKs spread on fibrinogen. Scale bars: 15  $\mu$ m; insets: 5  $\mu$ m.



**Supplemental Figure 5. Effects of platelet depletion on F-actin and β1-tubulin expression.**

(a) Platelet counts of mice treated with PBS (black line) or a platelet-depletion antibody (R300, grey line) were assessed over 144h. N = 5. Data is presented as mean ± SD. (b, c) Mean fluorescence integrity (MFI) of β1-tubulin was visualized and quantified in femoral cryosections derived from control or platelet-depleted mice. At least 50 cells were counted per group. Data is presented as mean ± SD. N = 4 mice. (d) Colocalization analysis for F-actin and septins was performed in MKs in femoral cryosections. Data is presented as mean ± SD. One dot represents one field of view containing several MKs.

## Supplemental Videos

**Video S1. Proplatelets are dynamic.** Proplatelets were isolated from the upper fraction of a density gradient performed on MKs 24h after the prior enrichment, treated with DMSO and embedded in methylcellulose. Timelapse images were acquired at a Lionheart automated microscope (Agilent Biotek). Scale bar: 100  $\mu\text{m}$ .

**Video S2. Actin depolymerization impairs proplatelet movement.** Proplatelets were isolated from the upper fraction of a density gradient performed on MKs 24h after the prior enrichment, treated with 10  $\mu\text{M}$  LatA and embedded in methylcellulose. Timelapse images were acquired at a Lionheart automated microscope (Agilent Biotek). Scale bar: 100  $\mu\text{m}$ .

**Video S3. Platelet bioreactor recapitulates proplatelet formation upon exposure to shear.** DMSO-treated, fetal liver-derived MKs were perfused into a custom microfluidic device<sup>6</sup> and proplatelet extensions into side channels were imaged using a Nikon Eclipse TE2000-E (10x objective) every 5 sec for 30 min. Scale bar: 150  $\mu\text{m}$ .

**Video S4. LatA impairs beading and release of proplatelet tips.** Fetal liver-derived MKs were perfused into a custom microfluidic device<sup>6</sup> and proplatelet extensions into side channels were imaged using a Nikon Eclipse TE2000-E (10x objective) every 5 sec. After 30 min, the syringe connecting to the channels was exchanged to media containing 30  $\mu\text{M}$  LatA to analyze existing proplatelet tips. MKs were imaged every 5 sec for another 30 min. Scale bar: 150  $\mu\text{m}$ .

**Video S5. FRAP imaging visualizing microtubule sliding in proplatelet shafts.** Proplatelets derived from MSCV- $\beta$ 1-tubulin-dendra2-transduced MKs were treated with DMSO and embedded in methylcellulose. FRAP was conducted by bleaching proplatelet regions with a 405 nm laser and imaging the FITC channel every sec for 1 min (20x objective; Yokogawa spinning disk confocal on an inverted Nikon Ti fluorescence microscope). Scale bar: 10  $\mu\text{m}$ .

**Video S6. Defective microtubule sliding visualized by FRAP imaging upon taxol treatment.** Proplatelets derived from MSCV- $\beta$ 1-tubulin-dendra2-transduced MKs were treated with 10  $\mu\text{M}$  taxol and embedded in methylcellulose. FRAP was conducted by bleaching proplatelet regions with a 405 nm laser and imaging the FITC channel every sec for 1 min (20x objective; Yokogawa spinning disk confocal on an inverted Nikon Ti fluorescence microscope). Scale bar: 10  $\mu\text{m}$ .

**Video S7. Unaltered microtubule sliding visualized by FRAP imaging upon LatA treatment.** Proplatelets derived from MSCV- $\beta$ 1-tubulin-dendra2-transduced MKs were treated with 10  $\mu\text{M}$  LatA and embedded in methylcellulose. FRAP was conducted by bleaching proplatelet regions

with a 405 nm laser and imaging the FITC channel every sec for 1 min (20x objective; Yokogawa spinning disk confocal on an inverted Nikon Ti fluorescence microscope). Scale bar: 10  $\mu\text{m}$ .

**Video S8. Dynamic actin foci in proplatelet shafts during proplatelet elongation.** Fetal liver-derived MKs were transduced with MSCV-LifeAct-mRuby and imaged every min for 30 min (20x objective; Yokogawa spinning disk confocal on an inverted Nikon Ti fluorescence microscope). Scale bar: 20  $\mu\text{m}$ .

**Video S9. Proplatelets are dynamic.** Proplatelets were isolated from the upper fraction of a density gradient performed on MKs 24h after the prior enrichment, treated with EtOH and embedded in methylcellulose. Timelapse images were acquired at a Lionheart automated microscope (Biotek). Scale bar: 100  $\mu\text{m}$ .

**Video S10. Septin inhibition hampers proplatelet movement.** Proplatelets were isolated from the upper fraction of a density gradient performed on MKs 24h after the prior enrichment, treated with 100  $\mu\text{M}$  FCF and embedded in methylcellulose. Timelapse images were acquired at a Lionheart automated microscope (Biotek). Scale bar: 100  $\mu\text{m}$ .

**Video S11. Actin-rich areas in proplatelet-forming MKs.** F-actin was visualized using 500 nM SiR-Actin and MKs were imaged over time using confocal microscopy (Leica LSM880, 40x objective). Scale bar: 30  $\mu\text{m}$ .

**Video S12. Static proplatelets upon actin inhibition.** Treatment with LatA attenuated proplatelet movement and reduced actin foci. SiR-Actin-stained MKs were imaged over time using confocal microscopy (Leica LSM880, 40x objective). Scale bar: 30  $\mu\text{m}$ .

**Video S13. Septin inhibition reduces actin foci.** MKs treated with 100  $\mu\text{M}$  FCF exhibit reduced motility and actin-rich nodules. MKs were imaged over time using confocal microscopy (Leica LSM880, 40x objective). Scale bar: 30  $\mu\text{m}$ .

## References

1. Kawamoto T, Shimizu M. A method for preparing 2- to 50-micron-thick fresh-frozen sections of large samples and undecalcified hard tissues. *Histochem Cell Biol.* 2000;113(5):331-339.
2. Vijey P, Posorske B, Machlus KR. In vitro culture of murine megakaryocytes from fetal liver-derived hematopoietic stem cells. *Platelets.* 2018;29(6):583-588.
3. Heib T, Gross C, Muller ML, Stegner D, Pleines I. Isolation of murine bone marrow by centrifugation or flushing for the analysis of hematopoietic cells - a comparative study. *Platelets.* 2020;1-7.
4. Bender M, Thon JN, Ehrlicher AJ, et al. Microtubule sliding drives proplatelet elongation and is dependent on cytoplasmic dynein. *Blood.* 2015;125(5):860-868.
5. French SL, Vijey P, Karhohs KW, et al. High-content, label-free analysis of proplatelet production from megakaryocytes. *J Thromb Haemost.* 2020;18(10):2701-2711.
6. Thon JN, Mazutis L, Wu S, et al. Platelet bioreactor-on-a-chip. *Blood.* 2014;124(12):1857-1867.
7. Nieswandt B, Bergmeier W, Rackebrandt K, Gessner JE, Zirngibl H. Identification of critical antigen-specific mechanisms in the development of immune thrombocytopenic purpura in mice. *Blood.* 2000;96(7):2520-2527.
8. Huang B, Wang W, Bates M, Zhuang X. Three-dimensional super-resolution imaging by stochastic optical reconstruction microscopy. *Science.* 2008;319(5864):810-813.
9. Rust MJ, Bates M, Zhuang X. Sub-diffraction-limit imaging by stochastic optical reconstruction microscopy (STORM). *Nat Methods.* 2006;3(10):793-795.
10. Wojcik M, Hauser M, Li W, Moon S, Xu K. Graphene-enabled electron microscopy and correlated super-resolution microscopy of wet cells. *Nat Commun.* 2015;6(7384).